Bulletin of Earthquake Engineering
https://doi.org/10.1007/s10518-023-01831-7

ORIGINAL ARTICLE

Fragility curves for the seismic assessment of masonry buildings in historic centres prone to out-of-plane failure modes

Valentina Cima[1] · **Valentina Tomei**[2] · **Ernesto Grande**[1] · **Maura Imbimbo**[2]

Received: 31 August 2023 / Accepted: 21 November 2023
© The Author(s), under exclusive licence to Springer Nature B.V. 2023

Abstract
The preservation and the safety of historic centers is certainly related to a large-scale assessment of the seismic vulnerability of their buildings. In this regard, fragility curves represent one of the most effective and widely used tools. Different methods, based on empirical, analytical and hybrid approaches, can be employed for deriving the fragility curves. Regarding the analytical-based fragility curves, their reliability is strongly influenced by the knowledge of the typological and structural features of the buildings, including constructive details, as well as by the evaluation of the seismic input, as evidenced in recent studies. This paper proposes an approach for evaluating the fragility curves of URM buildings towards OOP failure modes. The focus on OOP failure modes relies on the fact that in the past and more recent seismic events, most ordinary UnReinforced Masonry (URM) buildings in historic centres have shown to be particularly vulnerable to Out-Of-Plane (OOP) failure modes. The proposed approach combines the knowledge process concerning the typological and structural features of the buildings, with the analytical derivation of the fragility curves throughout an integrated multistep approach. In addition, the study also investigates the influence of the seismic input. The approach is discussed in detail in the first part of the paper and, in the second part of the paper, it is applied to the building stock of an Italian historic centre.

Keywords Analytical fragility curves · UnReinforced masonry buildings · Out-of-plane failure modes · Record-to-record variability · Historic centres · CARTIS forms

✉ Valentina Cima
v.cima@unimarconi.it

Valentina Tomei
v.tomei@unicas.it

Ernesto Grande
e.grande@unimarconi.it

Maura Imbimbo
m.imbimbo@unicas.it

[1] Department of Engineering Science, University Guglielmo Marconi, Via Plinio 44, 00193 Rome, Italy

[2] Department of Civil and Mechanical Engineering, University of Cassino and Southern Lazio, Via G. Di Biasio 43, 03043 Cassino, Italy

Published online: 12 December 2023

1 Introduction

Past and recent seismic events have shown that ordinary UnReinforced Masonry (URM) buildings in Italian and European historic centres are often highly susceptible to Out-Of-Plane (OOP) failure modes involving their façades (Giuffré 1993; Lourenço et al. 2011; Carocci 2012; Penna et al. 2014; Sorrentino et al. 2019; Vlachakis et al. 2020). In the framework of a large-scale seismic vulnerability assessment of these constructions, one of the most adopted and effective tools is represented by fragility curves (Lagomarsino and Cattari 2014; Ahmad and Ali 2017; Pelà 2018; Mosoarca et al. 2019; Moretić et al. 2023; Brando et al. 2017; Formisano 2017; Rapone et al. 2018; Chieffo et al. 2019, 2022; Chieffo and Formisano 2020; Liguori et al. 2023). Different methods can be employed for the derivation of fragility curves, ranging from empirical to analytical ones (Donà et al. 2020; Nale et al. 2021; Rosti et al. 2021; Sandoli et al. 2021, 2022; Shabani et al. 2021; Cima et al. 2023). Among these, empirical methods have been recently employed for the evaluation of the fragility curves for an Iranian historical centre (Biglari and Formisano 2020), while a comparison among the macroseismic approach, the Vulnus method and the mechanical non-linear macroelement analysis with the 3Muri software has been proposed in the context of the seismic assessment of a small town in the center of Italy (Chieffo and Formisano 2019). Regarding the analytical methods, the availability of the typological and structural data of the buildings (Tocchi et al. 2022) and the derivation of the seismic input (Silva et al. 2019) certainly represent two relevant aspects in the evaluation of the fragility curves. In particular, with reference to the OOP behavior of URM buildings in historic centres, the surveys done on the damages and collapses occurred after seismic events, have highlighted that the knowledge of the typological and structural features of the buildings, including constructive details, plays a fundamental role in identifying the potential OOP failure modes (D'Ayala and Speranza 2003; Saccucci et al. 2021). Moreover, regarding the modeling of the seismic input, the Italian code and the European guidelines allow for the use of spectral-shapes based on natural records as well as the adoption of smoothed spectra (D'Ayala et al. 2015). However, the use of natural records, unlike the employment of smooth code-based spectra, not only allows for selecting spectral shapes compatible with the seismicity of the site (Iervolino et al. 2010), but it also lets to evaluate the record-to-record variability, which is one of the major sources of uncertainty in the construction of fragility curves (D'Ayala et al. 2015; Banerjee et al. 2016; Baraschino et al. 2020; Nettis et al. 2021; Jalayer et al. 2021).

Aim of the present paper is to propose an approach that integrates a survey process of the buildings, composing the analyzed historic center, with an analytical approach for deriving the fragility curves. In particular, the survey process is addressed through both a qualitative and a quantitative approach, with different goals. The qualitative approach is devoted to identify, in each of the analyzed buildings, the most probable OOP mechanism on the basis of the main structural characteristics and details (such as chains, curbs, etc.); the quantitative approach aims to define buildings categories for each OOP failure mechanism and derive, for each category, the fragility curves. The scope of the proposal consists, then, in providing a tool to carry out a large-scale seismic vulnerability assessment of existing structures in function of the OOP failure mode that has the greatest probability of being activated in the building. The novelty of the proposal lies in the fact that, while others literature studies show fragility curves referring to both in-plane mechanisms and all OOP mechanisms (Ahmad and Ali 2017), in this paper the fragility curves are evaluated for each kind of the identified OOP mechanisms with the result of analyzing the different

level of vulnerability associated to each kind of the OOP mechanisms. The study represents an advancement of the approach presented by the Authors in previous works (Cima et al. 2021b, a, 2023). In particular, one of the main improvements consists of considering the influence of the record-to-record variability on the derivation of fragility curves by using spectrum-compatible natural records.

The approach could be a useful tool for municipalities technicians to plan an order of priorities for the retrofit interventions among the buildings composing the historic centers in order to safeguard their seismic safety.

The proposed approach is presented in detail in the first part of the paper. Then, in the second part, it is presented an application to the historic centre of Sora (central Italy). The latter, in particular, is carried out by employing both natural spectra, derived from combinations of spectrum-compatible recorded accelerograms, and smoothed spectra, provided by the Italian code (NTC 2018).

2 Integrated approach for deriving fragility curves at territorial scale

The proposed approach aims to derive the fragility curves for typologies of URM buildings characterizing a specific regional area and prone to the occurrence of OOP collapse modes. The approach is based on a multistep procedure which combines among them the knowledge process of the URM buildings typology with the numerical evaluation of the fragility curves. The approach, sketched in Fig. 1, is articulated into the following steps:

0. Define the building typologies representative of the area of study, being the building typology a set including ordinary buildings with similar structural-typological features and homogeneus in terms of age of construction (Zuccaro et al. 2015, 2023).
1. For each building typology, identify the most probable OOP failure modes of the URM buildings belonging to the typology. To this end, a qualitative analysis of the typological and constructive features of each building (knowledge process) influencing the activation of the OOP failure modes is carried out (Saccucci et al. 2021) as described in details in Sect. 2.1.

   It is important to highlight that the typologies constituted by low quality masonry buildings, where the activation of the OOP mechanisms is preceded by a masonry disaggregation, are not considered in this study since this aspect is beyond the scope of the paper, which refers to buildings susceptible to OOP mechanisms.
2. Subdivide the buildings of each typology into building categories, characterized by the same number of floors and the same most probable OOP failure mode; then generate sets of virtual buildings through the Monte Carlo procedure by varying the geometrical and mechanical parameters affecting the identified OOP failure modes.
3. For each building category, evaluate the capacity curve of the virtual buildings composing the category throughout a non-linear kinematic analysis (Casapulla and Argiento 2017; ISR 2019; Cima et al. 2021a).
4. Evaluate the seismic demand in terms of the spectra obtained from the spectrum-compatible natural accelerograms.
5. Define the Damage Indexes, DI_{DSi}, for rigid block mechanisms (Lagomarsino 2015) related to the moderate damage DS1, corresponding to the activation of the OOP failure modes at the Damage Limit State, and the complete damage DS2, corresponding to achievement of the Safeguard Life Limit State (ISR 2019).

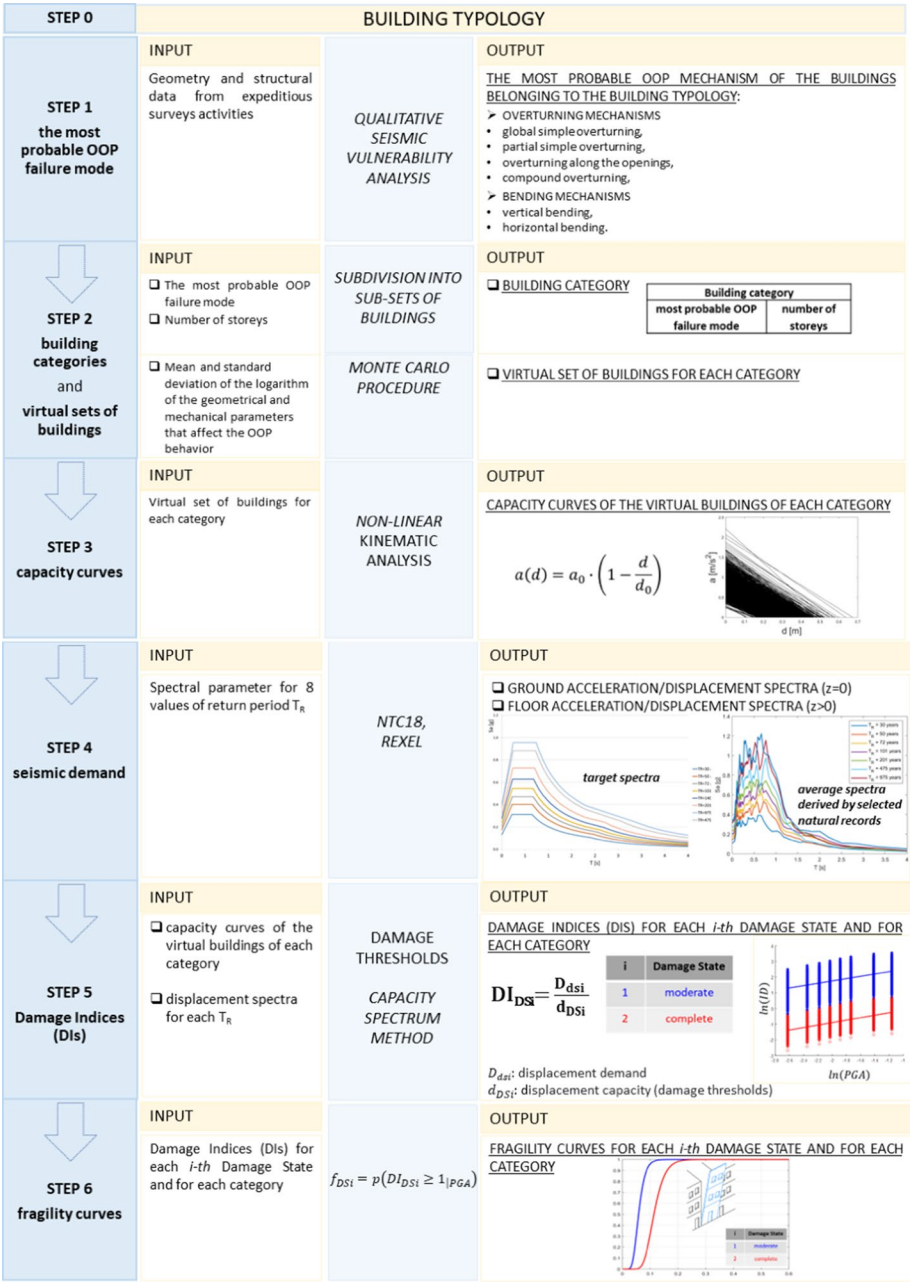


Fig. 1 Schematic description of the steps of the proposed approach

6. Derive the fragility curves for each damage state, DS1 and DS2, and for each building category.

Each step is discussed in detail in the following sub-sections.

2.1 Typologies and virtual sets of buildings (categories)

The ordinary buildings belonging to the area of study are, preliminary, clustered into building typologies (step 0), being the building typology a set including buildings with homogeneous construction ages and similar structural-typological features, in terms of type of masonry, slabs, vaults, roof, past structural interventions, intended use, number of storeys and average height of storeys (Zuccaro et al. 2015, 2023).

Then, the proposed approach proceeds, in step 1, with a qualitative analysis of the buildings belonging to the typologies representative of the area under study. It is indeed finalized to identify, for each building of each typology, the most probable OOP failure mode in case of earthquake event (Saccucci et al. 2019, 2021; Saccucci 2020). Such analysis requires a preliminary process of knowledge, aimed to collect data which allow to identify the most likely OOP failure modes involving the local seismic response of the perimeter façade of the building. To this end, the qualitative analysis requires, as input, the geometric, structural and constructive data. Among these, a particular relevance is devoted to the dimensions of the façade wall, the distribution of openings, the presence of tympanum, the structural details and connections among orthogonal walls and among floors and walls (i.e. curbs, chains, tie rods, toothing between perpendicular walls, etc.). These data can be obtained through surveys on sight supported by historical archival researches (real estate registry cartographies, project documents related to the original construction of the building and to any subsequent interventions, etc.); useful information can be also obtained by consulting databases that report the typological-structural characteristics of the national building heritage or by using web mapping tools available online, such as Google Maps, Google Street View and Bing Maps, widely used both in crowd-sourcing approaches (Scaini et al. 2022) and for the creation of exposure database to support the seismic vulnerability assessment of existing buildings (Columbro et al. 2022).

The collected information allows for the evaluation of the most probable OOP failure modes of the analyzed buildings. Indeed, the construction weaknesses, emerged from the knowledge process, can be related to the occurrence of specific OOP failure modes of the perimeter facades composing the building (Zuccaro and Rauci 2008; Saccucci et al. 2021). More in details, the qualitative analysis requires as input the following data (Saccucci 2020):

- Geometrical characteristics of the façade wall (number of floors, presence of tympanum, discontinuity of wall sections, façade length and slenderness);
- Geometrical characteristics of openings (number of openings for each floor, dimensions of openings, presence of openings vertically aligned);
- Structural and constructive features (toothing between perpendicular walls, presence of vaulted floors, typology of slabs, slab warping, masonry type, presence of chains and tie rods, presence of curbs).

On the base of the presence/absence of specific vulnerability factors, such as low slenderness, tympanum, interfloor connections, curbs, chains, tie rods, aligned holes,

discontinuity of wall sections and large spans between the walls orthogonal to the façade, the qualitative analysis associates the most probable OOP mechanism to each building.

For example, the global simple overturning of a façade wall results the most probable failure mode in the case the façade is not effectively connected with the orthogonal walls and the slabs (Fig. 2a). Conversely, in presence, at the lower floors, of an effective toothing between the façade and the transverse walls, the most likely failure mode results the partial overturning of the upper levels (Fig. 2b) Then, if the façade is connected to the orthogonal walls, but the openings are aligned, a global simple overturning along opening is associated (Fig. 2c).

Based on the results of the qualitative analysis, in terms of the most probable OOP failure mode, the buildings of each typology are clustered into categories, characterized by the same number of floors and the same most probable local failure mode. Therefore, while the building typologies include buildings with similar structural-typological features, the categories are subsets of the single typology, distinguished by the most probable OOP mechanism and the specific number of floors.

Then, the approach proceeds with the step 2 developed with reference only to the categories of buildings prone to the global simple overturning, the partial overturning and the global simple overturning along openings (Fig. 2), which generally represent the mechanisms most frequently observed in historical centres after a strong earthquake (D'Ayala and Speranza 2003). According to the step 2, for each category of the buildings prone to the overturning mechanisms, virtual populations of buildings are generated in order to take into account the uncertainties due to the intrinsic variability of the mechanical and geometric properties which affect the OOP capacity of the buildings (Cima et al. 2021b). In particular, virtual buildings are generated through a Monte Carlo procedure, by varying the wall thickness s, the story height h, the percentage of holes in the façade b and the compressive strength of the masonry f_c. For each considered parameter, a lognormal distribution with mean and standard deviation defined on the basis of the sample values or defined according to the values available in the literature is assumed; this type of statistical distribution is, indeed, generally used to represent aleatory variables varying in the range $0, +\infty$ (Park et al. 2009; CNR-DT212. 2013; Simões et al. 2020; Giordano et al. 2021).

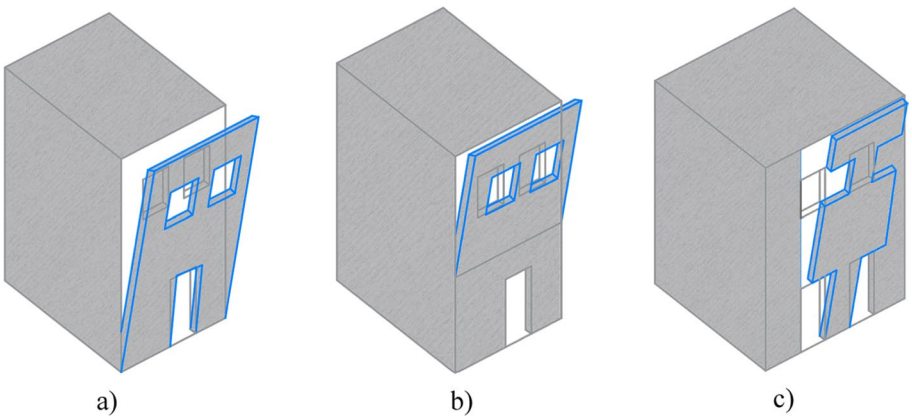


Fig. 2 Types of OOP failure modes considered in the study: **a** global simple overturning; **b** partial overturning; **c** global simple overturning along opening

2.2 Capacity curves

The step 3 of the proposed approach consists of evaluating the capacity curves of each virtual building belonging to each category. These curves report the spectral acceleration "a" corresponding to the multiplier of horizontal seismic forces vs the spectral displacement "d" corresponding to the displacement at the top of the façade during the evolution of the OOP failure mode. The curves are deduced by performing the well-known nonlinear kinematic analysis of the wall portion involved in the failure mode, under the following hypotheses: rigid block mechanism, no-tensile masonry material with limited compression strength (Lagomarsino and Resemini 2009), absence of sliding between blocks (ISR 2019; Heyman 2014). In particular, in order to take into account the limited compressive strength of the masonry, the position of the hinge, i.e. the point around which the façade rotates during the evolution of the mechanism, is set back from the end of the section of a quantity *t* evaluated through the following equation (Lagomarsino and Resemini 2009):

$$t = \frac{\sum W_i}{2 \cdot \alpha_c \cdot l \cdot f_c} \tag{1}$$

where $\sum W_i$ is the total weight of the wall, α_c is a reduction coefficient of compressive strength equal to 0.85 (ISR 2019), l is the length of the hinge and f_c is the value of the compressive strength.

2.3 Seismic demand

The step 4 is finalized to derive the seismic demand in terms of the displacement spectra. To this purpose, the spectra are derived starting from the combinations of natural spectra, which are selected by imposing the compatibility with the target spectra of the site, related to the analyzed regional area under study, through the software REXEL (Iervolino et al. 2010) (available at http://www.reluis.it/). In particular, the target spectra are defined according to the Italian Code for eight different return periods TR (30, 50, 72, 101, 140, 201, 475, 975 years). Compatibility is imposed on the acceleration target spectra in order to have an average spectrum derived by the natural records included, for the periods of interest, within the tolerance range − 10%/ + 30% (Fig. 3).

In case of the failure mode activated at the ground floor of the building (z = 0), the range of periods of interest of the collapse mode is assumed equal to the range of the characteristic periods of the local mechanism, T_k (ISR 2019) given by:

$$T_k = 2\pi\sqrt{\frac{0.8 \cdot d_{DSi}}{a\left(0.8 \cdot d_{DSi}\right)}} \tag{2}$$

where $a(0.8 \bullet d_{DSi})$ is the spectral acceleration corresponding to a level of displacement equal to $0.8 \bullet d_{dSi}$ in the capacity curve and d_{DSi} is the threshold damage corresponding at the i-th damage state, as defined in the step 5 of the proposed approach.

Differently, in case of the failure mode activated at the upper floors of the building (z > 0), since the seismic demand depends on the fundamental period of the structure, the compatibility is directly imposed in the range of the fundamental period T_1 of the analyzed building.

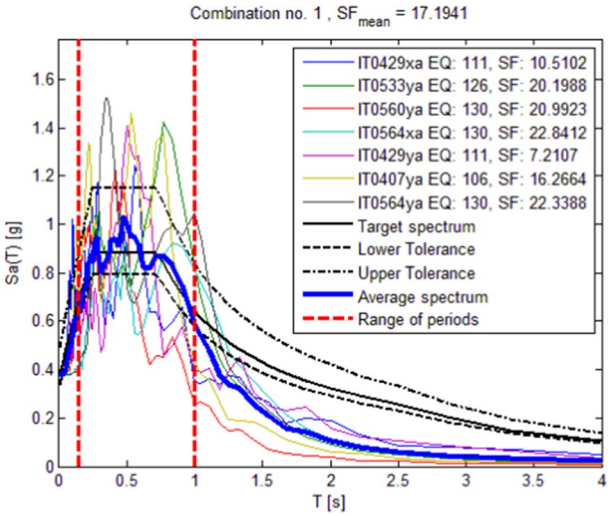


Fig. 3 Example of combination of natural spectra compatible with a site target-spectrum provided by REXEL

For the moderate damage, corresponding to the activation of the OOP failure mode (ISR 2019) as discussed in details in Sect. 2.4, the fundamental period of the structure can be assumed equal to the elastic periods T_{1el} evaluated according to the following equation (European Commitee for Standardization 2004):

$$T_{1el} = 0.05 \cdot H^{3/4} \tag{3}$$

where H is the height of the building expressed in m.

For the complete damage, corresponding to the achievement of the Safeguard Life Limit State (ISR 2019), the periods T_1 can be deduced from the equation proposed by (Abbati et al. 2018), which takes into account the level of ductility reached by the structure due to the nonlinear behavior, that is:

$$T_1 = \frac{1 + \sqrt{\mu}}{2} \cdot T_{1el} \tag{4}$$

where μ is the maximum ductility demand which, according to the study reported in (Abbati et al. 2018) can be assumed equal to 3.3.

In order to account for the record-to-record variability (step 6), in addition to the average spectrum, also the 84th and the 16th percentile of the selected records are considered.

Starting from these spectra in terms of the acceleration both the ground displacement and the floor displacement spectra are evaluated in compliance with the Italian Code and Seismic Recommendation (NTC18 2018; ISR 2019). In particular, for the evaluation of the floor spectra, the following parameters are considered:

- An equivalent viscous damping of the OOP mechanism ξ equal to 0.05, for the DS1, and equal to 0.08, for the DS2 (ISR 2019);
- An equivalent viscous damping of the structure ξ_1 equal to 0.05, for the DS1, whereas, for the DS2, the ones given by the following expression (Calvi 1999; Blandon and Priestley 2005):

$$\xi_{1DS2} = \xi_{1e} + \xi_H \cdot \left(1 - \frac{1}{\mu^\beta}\right) \tag{5}$$

where ξ_{1e} is the elastic viscous damping of the structure, assumed to be 0.05, ξ_H is the maximum hysteretic contribution assumed equal to 0.10, μ is the ductility level of the structure assumed equal to 3.3 (Abbati et al. 2018) and β is a factor depending on the hysteretic properties of the structure, assumed equal to 0.5.

The evaluation of the dispersion due to the record-to-record variability is described in Sect. 2.4.

2.4 Damage indices and fragility curves

The fragility curves are derived with reference to two damage states DS: DS1 (*moderate*) and DS2 (*complete*), corresponding respectively to the activation of the OOP mechanism for the achievement of the Damage Limit State and the collapse due to the achievement of the Safeguard Life Limit State. To this end, a Damage Index, DI_{DSi}, defined in terms of the ratio between the maximum displacement demand for a given damage state, namely D_{DSi}, and the corresponding damage threshold, namely D_{DSi}, is introduced (step 5 of the procedure).

The maximum displacement demand is evaluated through the Capacity Spectrum Method CSM (Freeman 1998) by using the ground displacement spectra, in the case the OOP mechanism occurs at the base of the ground floor of the building ($z = 0$), the floor displacement spectra in the case the OOP mechanism occurs at the base of the upper floors ($z > 0$) (ISR 2019).

On the other hand, since the damage states are defined in correspondence of the Limit States suggested by the Italian Code (See Fig. 4), the threshold of the *moderate* damage state, DS1, is assumed equal to:

$$d_{DS1} = d_y \tag{6}$$

where d_y is the spectral displacement related to the Damage Limit State SLD, corresponding to the intersection between the capacity curve of the mechanism and a pseudo-elastic linear branch given by the following equation (Lagomarsino 2015):

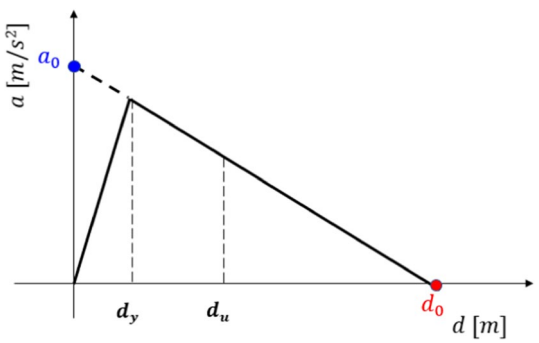


Fig. 4 The damage thresholds of the considered damage states

$$a(d) = \frac{4 \cdot \pi^2}{T_e^2} d \tag{7}$$

where T_e represents the initial pseudo-elastic period of the mechanism. The latter can be estimated approximately through the following formula (ISR 2019):

$$T_e = k \cdot \lambda \cdot L \sqrt{\frac{\gamma}{E \cdot g}} \tag{8}$$

where: k is a coefficient assumed to equal to 6.2 (ISR 2019); L is the length of the wall; λ is the slenderness of the wall; γ is the masonry specific weight; E is the elastic modulus of the masonry and g is the gravity acceleration.

Such branch is introduced in order to take into account the elastic behavior of the wall before the activation of the OOP mechanisms (Candela et al. 2013; Lagomarsino 2015).

Regarding the second damage state, DS2, it is related to the Safeguard Life Limit State, SLV. Consequently, it results:

$$d_{DS2} = d_u \tag{9}$$

being:

$$d_u = 0,4 \cdot d_0 \tag{10}$$

where d_0 is the spectral displacement corresponding to a spectral acceleration equal to zero.

Finally, step 6 proceeds with the evaluation of the fragility curves. To this purpose, considering the Peak Ground Acceleration, PGA, as an indicative parameter of the intensity of the seismic input and assuming a log-normal distribution of the DI_{Dsi}, conditioned on a given value of PGA, the following equation is used for deriving the fragility curves for each damage state (CNR-DT212 2013):

$$F_{DSi} = p\left(DI_{Dsi} \geq 1_{|PGA}\right) = 1 - \Phi\left(\frac{\ln 1 - \mu_{\ln DI_{Dsi|PGA}}}{\sigma_{\ln DI_{Dsi|PGA}}}\right) = \Phi\left(\frac{\mu_{\ln DI_{Dsi|PGA}}}{\sigma_{\ln DI_{Dsi|PGA}}}\right) \tag{11}$$

where:

- $\Phi[\bullet]$ is the lognormal standard cumulative density function (CDF),
- $\mu_{\ln DIiIPGA}$ is the mean value of the natural logarithm of the variable DI_{Dsi} conditioned on the given value of PGA,
- $\sigma_{\ln DIiIPGA}$ is the total dispersion of the natural logarithm of the variable DI_{Dsi} conditioned on the given value of PGA.

In this paper, the conditional mean values of the natural logarithm of the variable DI_{Dsi} are defined by performing a linear regression of the logarithm of the damage indices, obtained in the step 5, versus the logarithm of the values of PGA used for the evaluation of the seismic demand in the step 4 (see Fig. 5). From the regression, indeed, it is possible to estimate the mean value of the logarithm of the limit state variable DI_{DSi} conditioned on the level of PGA through the expression (Nielson and DesRoches 2007):

$$\mu_{\ln DI_{Dsi|PGA}} = A_{Dsi} + B_{Dsi} \cdot \ln(PGA) \tag{12}$$

where A_{DSi} and B_{DSi} are coefficients obtained by the linear regression.

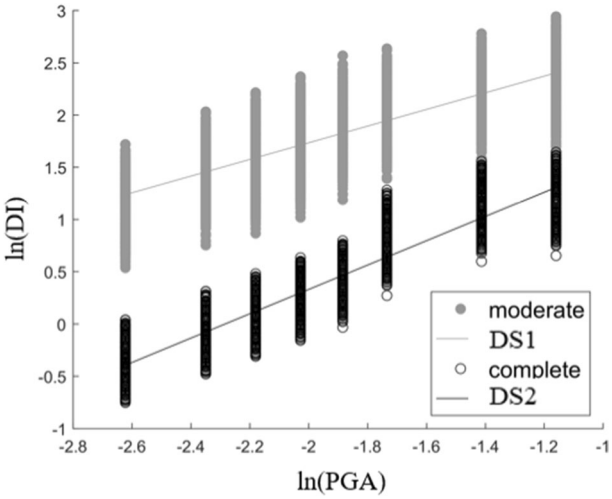


Fig. 5 Example of linear regression of the logarithm of DI versus the logarithm of the PGA

Concerning the total dispersion, two sources of uncertainty (Applied Technology Council 2012) are considered for deriving the fragility curves:

- The modelling uncertainty σ_{mDSi}, which takes into account for the variability of the actual characteristics of the buildings as well as the variability of the accuracy of the analytical model adopted to capture the behavior of the buildings; consequently, it depends on the geometry and mechanical properties of the façade walls as well as on the considered seismic demand;
- The record-to-record uncertainty σ_{rtrDSi} related to the variability of the natural seismic records (D'Ayala et al. 2015).

The modelling uncertainty values are estimated by applying the following relation (Jalayer et al. 2015):

$$\sigma_{mDSi} = \sqrt{\frac{\left(\sum_{i}^{nPGA} \ln DI_{DSi} - \mu_{\ln DI_{DSi|PGA}}\right)^2}{n-2}} \tag{13}$$

where nPGA is the number of PGA considered for the evaluation of the seismic input, DI_{DSi} is the i-th damage state evaluated by considering the average spectra of the selected records and n is the number of the generated virtual buildings.

The record-to-record dispersions are estimated through the following formula (Lagomarsino and Cattari 2014):

$$\sigma_{rtrDSi} = \frac{1}{2} \cdot \left| \overline{\ln DI_{DSi\ 16}} - \overline{\ln DI_{DSi\ 84}} \right| \tag{14}$$

where $\overline{\ln DI_{16}}$ and $\overline{\ln DI_{84}}$ are the mean values of the natural logarithm of the i-th damage indices evaluated by considering the 16th and the 84th percentile of the selected records, respectively.

Then, the total dispersion values are evaluated by combining the modelling uncertainty and the record-to-record uncertainty through the following expression:

$$\sigma_{\ln DI_{DSi|PGA}} = \sqrt{\sigma^2_{mDSi} + \sigma^2_{rtrDSi}} \tag{15}$$

3 Application of the proposed approach to the case study of historic centre of Sora

The proposed approach has been applied to the URM building typologies characterizing the historic centre of Sora. The typologies have been identified by using the survey forms developed in the context of the research project CARTIS (DPC/ReLUIS 2019–2021 and 2022–2024), a project granted by the Italian Department of Civil Protection and ReLUIS (Network of the Italian University Laboratories for Seismic Engineering) with the main objective of creating a database of the structural and typological features characterizing the ordinary buildings typical of Italian Municipalities. More in details, according to the user's manual provided by CARTIS project (Protezione Civile 2017), each examined Municipality is divided into homogeneous areas in terms of the age of construction and construction techniques; the survey forms summarize the main structural and typological features of the prevalent building typologies in each homogeneous area, in terms of the following parameters: number of storeys, average height of storeys, characteristics of the masonry, slabs, vaults, roof and structural interventions (Zuccaro et al. 2015).

In detail, the information required to fill the CARTIS forms was obtained by the Authors through on-site inspections, by using online resources, such as Google Maps and Google Street View, and consulting design drawings and archive documents at the municipal archives of Sora.

From the collected data, two prevalent URM building typologies have been identified in the historic centre of Sora (Fig. 6a), named "MUR 1" and "MUR 2" (see Fig. 6b) and described in details in Table 1.



Fig. 6 Historic centre of Sora: **a** top view; **b** plan view with identification of the building typologies detected by the CARTIS forms

Table 1 Features of the building typologies identified in the historic centre of Sora

Building typology	MUR 1	MUR 2
Masonry type	Irregular masonry with rough stones	Regular masonry with square stones
Construction age	< 1860	1861–1945
Number of storeys	2–3	2–3
Average height of storeys	2.5–3.49 m	2.5–3.49 m
Intended use	Residential use, storage use	Residential use, commercial use, storage use
Slabs	Made of wood, mainly oriented parallel to the façade	In hollow core concrete, mainly oriented parallel to the façade
Roof	Gabled roof, mainly oriented parallel to the façade	Gabled roof and flat roof, mainly oriented parallel to the façade
Materials of the roof	Timber and reinforced concrete	Timber and reinforced concrete

Table 2 Building categories identified in the historic centre of Sora

Building category	OOP failure mode	Number of storeys
GO3	Global simple overturning	3
PO2_2	Simple partial overturning of the 2nd level	2
PO3_3	Simple partial overturning of the 3rd level	3
PO3_2-3	Simple partial overturning of the 2nd and the 3rd level	3
GOAO2	Global overturning along the opening	2
GOAO3		3
HB2	Horizontal bending	2
HB3		3
VB2	Vertical bending	2
VB3		3

Table 3 Values of mean and standard deviation used to generate the virtual sets of buildings

Parameter	Floor of the buildings	MUR 1		MUR 2	
		Mean	Standard deviation	Mean	Standard deviation
s	1st	− 0.35	0.17	− 0.41	0.11
	2nd	− 0.44	0.20	− 0.51	0.08
	3rd	− 0.48	0.20	− 0.60	0.08
h	1st	1.08	0.21	1.16	0.16
	2nd	1.07	0.13	1.10	0.06
	3rd	1.01	0.26	1.07	0.10
b	1st	− 0.62	0.17	− 0.52	0.11
	2nd	− 0.19	0.09	− 0.20	0.11
	3rd	− 0.26	0.12	− 0.31	0.13

As it can be deduced from Table 1, the two typologies differ in terms of construction age and masonry type, but they are characterized by similar features in terms of number of storeys, average height of storeys, intendeduse, features of slabs and roof.

In particular, the application of the step 1 of the approach detects, for each building typology, five types of the most probable OOP failure modes (see Table 2) namely the global simple overturning, the simple partial overturning, the global overturning along the opening, the horizontal bending and the vertical bending.

Then, on the basis of these results, the buildings of the two typologies have been subdivided into ten building categories, characterized by the same number of storeys and the same most probable OOP failure mode, as reported in Table 2: one category for the global simple overturning named "GOi"; three categories for the simple partial overturning named "POi_j"; two categories for the global overturning along the openings named "GOAOi"; two categories for the horizontal bending named "HBi" and two categories for the vertical bending named "VBi". The index "i" in the labels of categories indicates the number of floors of the buildings belonging to the considered category, while "j" indicates the floors involved in the simple partial overturning failure modes.

Then, for each category, virtual populations of 3000 buildings have been generated through the Monte Carlo Method, by assuming a lognormal distribution for the values of both geometrical and mechanical parameters. In particular, the geometrical parameters have been generated by using the mean and the standard deviation values shown in Table 3; these values represent, for each floor of the sample buildings belonging to the two typologies, the mean and the standard deviation of the values of the parameters *s*, *h* and *b*, characterizing the sample buildings belonging to the two typologies "MUR 1" and "MUR 2" and obtained by the project drawings and the archive documents consulted in the archives of the Municipality. On the other hand, the values of the compressive strength of the masonry have been generated by considering the mean and the standard deviation values characterizing the masonry types of the examined typologies, reported in (CNR-DT212 2013).

According to the step 3 of the proposed approach, for each category, the wall portion involved in the failure mode of each virtual building has been analyzed to obtain the corresponding capacity curve.

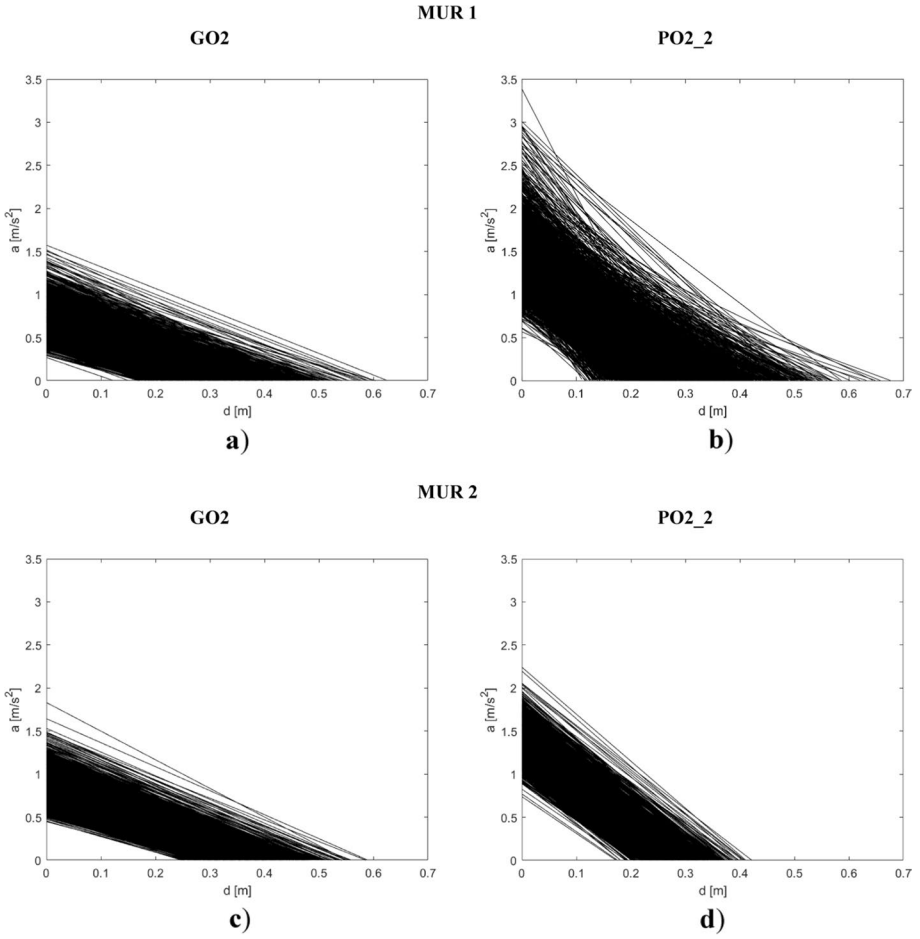


Fig. 7 Capacity curves of the building category: **a** GO2 belonging to "MUR 1"; **b** PO2_2 belonging to "MUR 1"; **c** GO2 belonging to "MUR 2"; **d** PO2_2 belonging to "MUR 2"

Figure 7 shows, as an example, the capacity curves obtained for the buildings of the categories GO2 and PO2_2 belonging to both the typologies "MUR 1" and "MUR 2". The plots clearly underline the ranges of variation of the displacement capacity (last point of the capacity curves) and the spectral acceleration corresponding to the activation of the mechanism particularly dependent on the type of failure mode.

After the evaluation of the capacity curves, for each considered damage state DS and for each investigated building category, eight combinations of seven spectra, each of them derived by natural records, have been selected through the software REXEL (Iervolino et al. 2010). The selection has been made by imposing the compatibility with respect to the target spectra defined for the site of the historic centre of Sora in compliance with the NTC18. In particular, the target spectra have been derived, for eight values of the return period T_R varying between 30 and 975 years, by considering a topographical category T1 (corresponding to the case of soil configuration) and a subsoil category equal to D (the latter deduced from the Geological Map of Sora and the tables of the Macro Homogeneous Areas in Seismic Perspective, created as part of the Level 1 Seismic Microzonation Plan of the Municipality of Sora).

For each combination, the average, the 84th and the 16th percentile spectra of the selected records have been derived. Then, starting from these spectra in terms of acceleration (of which an example is given in Fig. 8), both the ground displacement spectra and the floor displacement ones have been derived.

Subsequently, the damage thresholds, the maximum demands required to the failure modes and the related damage indices, DI_{Dsi}, have been deduced according to step 5, for each category and for both the damage states.

To assess the influence of the type of the selected spectra on the fragility curves, the last step has been carried out by using both the selected natural spectra and the smoothed spectra deduced from the national Code. In particular, the same values of dispersion related to the record-to-record variability, σ_{rtrDSi}, have been considered for both spectrum types. Table 4 reports the dispersions related to the record-to-record variability σ_{rtrDSi}, and to the modelling dispersions σ_{mDSi}. From the data reported in Table 4 emerges that, while the dispersion due to the record-to-record variability σ_{rtrDSi} is the same for both spectra, the modelling dispersion σ_{mDSi} differs because of its dependance on the spectral shape.

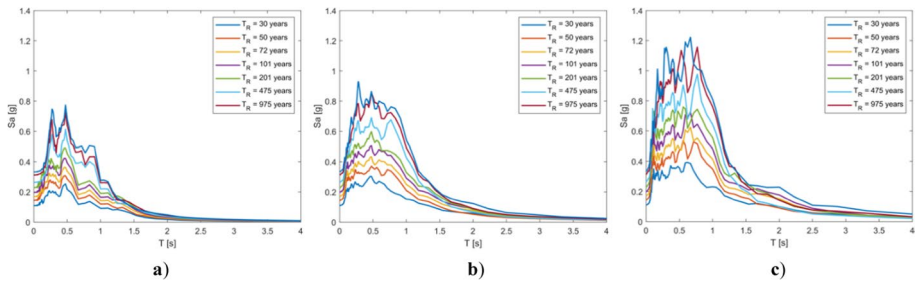
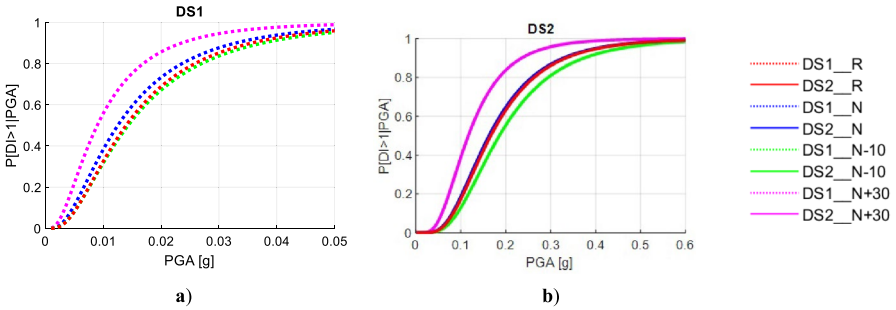


Fig. 8 Example of: **a** the 16th percentile spectra of selected records; **b** the average spectra of the selected records; **c** the 84th percentile spectra of the selected records

Table 4 Values of the dispersion σ_{rtrDSi} and σ_{mDSi}

Building typology	Building category	NTC				REXEL			
		σ_{rtrDS1}	σ_{rtrDS2}	σ_{mDS1}	σ_{mDS2}	σ_{rtrDS1}	σ_{rtrDS2}	σ_{mDS1}	σ_{mDS2}
MUR 1	GO2	0.3106	0.5524	0.1624	0.2092	0.3106	0.5524	0.2561	0.2105
	GOAO2	0.2855	0.5941	0.1852	0.206	0.2855	0.5941	0.2953	0.2113
	PO2_2	0.3138	0.1901	0.4598	0.3198	0.3138	0.1901	0.4661	0.3164
MUR 2	GO2	0.2521	0.548	0.1084	0.1355	0.2521	0.548	0.2319	0.1391
	GOAO2	0.2533	0.598	0.1484	0.137	0.2533	0.598	0.2367	0.1369
	PO2_2	0.3004	0.1953	0.3182	0.2054	0.3004	0.1953	0.3228	0.1888
MUR 1	GO3	0.3949	0.6314	0.2288	0.2892	0.3949	0.6314	0.2436	0.3073
	GOAO3	0.383	0.6544	0.1859	0.2377	0.383	0.6408	0.2034	0.2556
	PO3_2-3	0.1800	0.2819	0.4812	0.3274	0.1800	0.2819	0.4875	0.3656
	PO3_3	0.1764	0.2861	0.56453	0.3265	0.1764	0.2861	0.5739	0.3607
MUR 2	GO3	0.3496	0.6409	0.138	0.1303	0.3496	0.6409	0.1578	0.1604
	GOAO3	0.3558	0.6575	0.1484	0.137	0.3558	0.6425	0.1607	0.1664
	PO3_2-3	0.1587	0.2848	0.32843	0.215	0.1587	0.2848	0.3349	0.2666
	PO3_3	0.1575	0.2847	0.3468	0.1698	0.1575	0.2847	0.3543	0.2188



a) b)

Fig. 9 Fragility curves for the category PO3 be part of the structural typology "MUR 1": **a** damage limit state DS1; **b** damage limit state DS2

3.1 Results and discussion

The fragility curves obtained with reference to the selected case study are reported in Figs. 9, 10, 11, 12 and 13.

In particular, Fig. 9 shows the fragility curves for the category of the three-story buildings, be part of "MUR 1", subjected to the simple partial overturning of the third floor (PO3). It can be observed that:

- The curves DS1_R and DS2_R are the ones obtained by considering the spectral shapes derived by natural accelerograms (REXEL), for *moderate* damage DS1 (Fig. 9a) and *complete* damage DS2 (Fig. 9b), respectively; in this case, the record-to-record variability has been evaluated by means of the dispersion σ_{rtrDSi} referred to the natural records;

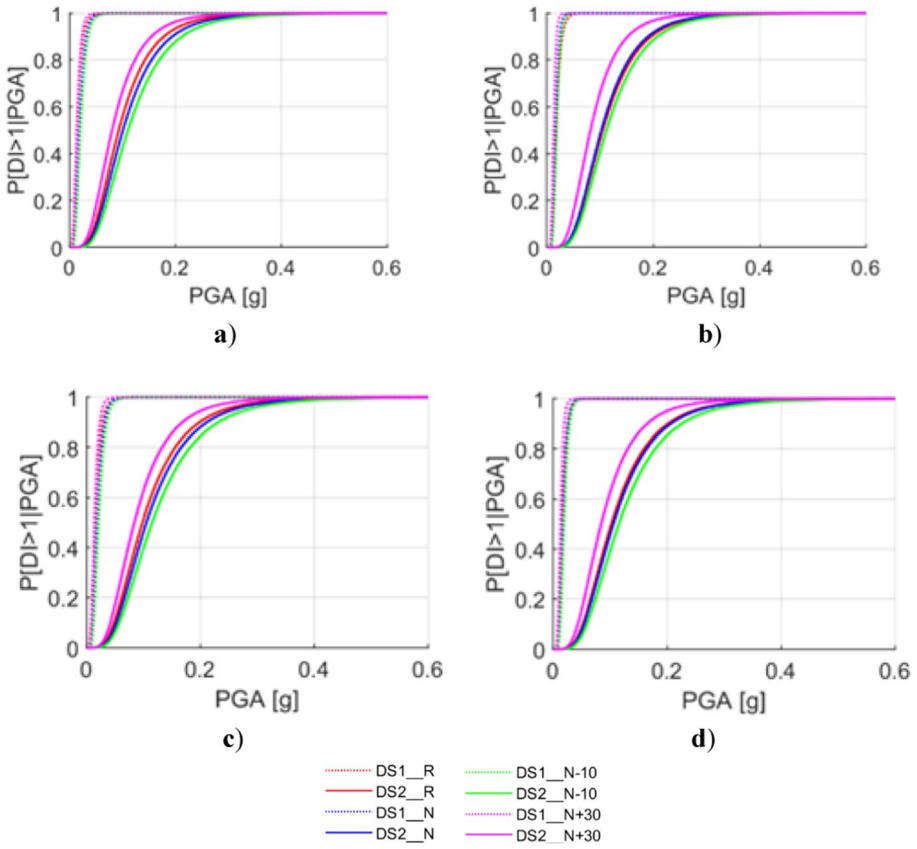


Fig. 10 Fragility curves for the categories of the two-story buildings prone to: **a** global overturning—"MUR 1"; **b** global overturning—"MUR 2"; **c** global overturning along openings—"MUR 1"; **d** global overturning along openings—"MUR 2"

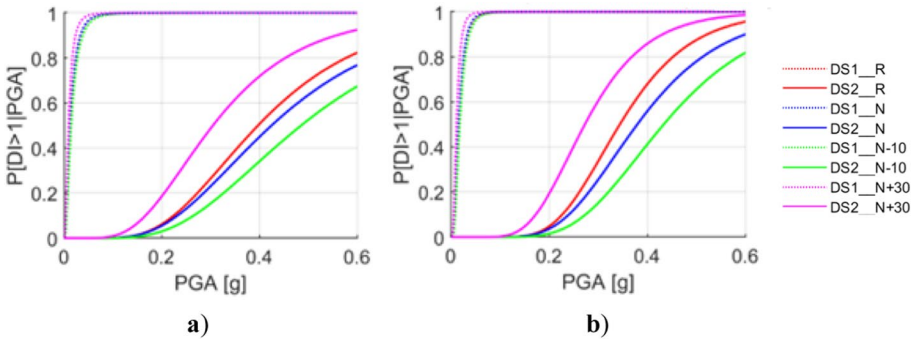


Fig. 11 Fragility curves for the categories of the two-story buildings, be part of the two building typologies "MUR 1" (**a**) and "MUR 2" (**b**), prone to partial overturning

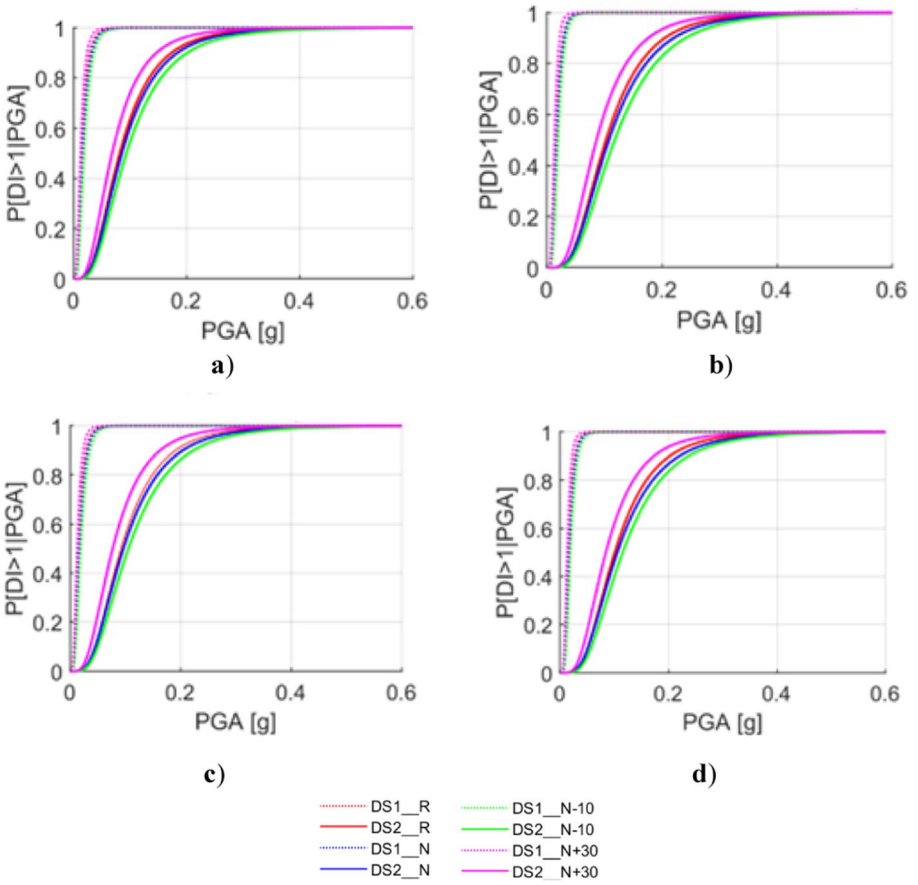


Fig. 12 Fragility curves for the categories of the three-story buildings, be part of the two building typologies "MUR 1" and "MUR 2", prone to: **a** global overturning– "MUR 1"; **b** global overturning– "MUR 2"; **c** global overturning along openings—"MUR 1"; **d** global overturning along openings—"MUR 2"

- The curves DS1_N and DS2_N are the ones obtained by considering the smoothed spectra proposed by the Italian code (NTC 18) for *moderate* damage DS1 (Fig. 9a) and *complete* damage DS2 (Fig. 9b)), respectively, and still adopting the dispersion σ_{rtrDSi} referred to the natural records;
- The curves DS1_N-10 (Fig. 9a) and DS2_N-10 (Fig. 9b) are the ones obtained by considering the smoothed spectra proposed by the Italian code (NTC 18) reduced by 10% for the two damage levels DS1 and DS2, respectively. The adopted dispersion is σ_{rtrDSi};
- The curves DS1_N + 30 (Fig. 9a) and DS2_N + 30 (Fig. 9b) are the ones obtained by amplifying the smoothed spectra proposed by the Italian code (NTC 18) by 30% (the range − 10% and + 30% identifies the lower and upper boundaries of the range of tolerance suggested by the Italian code for selecting natural accelerograms spectrum-compatible). The adopted dispersion is σ_{rtrDSi}.

It is important to underline that, although the DS1_R (DS2_R) and DS1_N (DS2_N) fragility curves have been deduced by assuming the same value of the dispersion related to

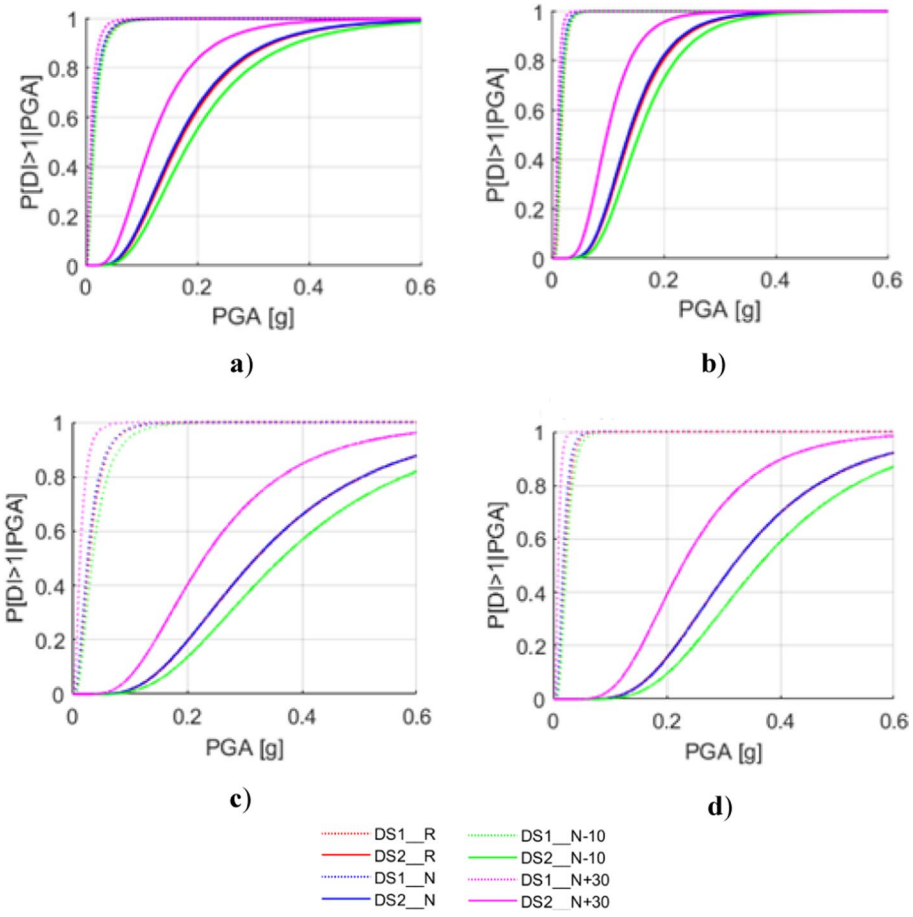


Fig. 13 Fragility curves for the categories of the three-story buildings, be part of the two building typologies "MUR 1" and "MUR 2", prone to: **a** partial overturning of the 3rd floor—"MUR 1"; **b** partial overturning of the third floor—"MUR 2"; **c** partial overturning of the 2nd and 3rd floor—"MUR 1"; **d** partial overturning of the second and third floor—"MUR 2"

the record-to-record variability σ_{rtrDSi}, they are characterized by different values of both the modelling dispersion σ_{mDSi} and the conditional mean value $\mu_{lnDIi|PGA}$; these values, indeed, depend on the damage thresholds and on the maximum displacement demands requested to the failure modes. The damage thresholds are deduced from the capacity curves, therefore are the same in both cases, but the maximum displacement demands change in the two different cases since they depend on the spectra.

By comparing the fragility curves obtained from natural accelerograms (DS1_R and DS2_R) and those obtained from smoothed spectra (DS1_N and DS2_N), at the same Limit State, it is possible to observe that the curves lead to similar levels of fragility (i.e. similar values of probability to attain the selected limit state) and both lie between the two curves DS1_N-10 (DS2_N-10) and DS1_N + 30 (DS2_N + 30). This points out that, for the categories of three-story buildings, be part of "MUR 1", subjected to the simple partial overturning of the third floor (PO3), the different values of the modelling

dispersion and the conditional mean value do not play a significant role on the fragility curves obtained by considering either natural accelerograms or smooth code-based design spectra.

Figures 10, 11, 12 and 13 show the curves DS1_R, DS2_R, DS1_N and DS2_N for the building categories detected for the two typologies ("MUR1" or "MUR2") not analyzed in Fig. 9.

In particular, the curves reported in Fig. 10 refer to the categories of the two-story buildings, be part of "MUR 1" and "MUR 2", prone to global overturning (Fig. 10a and b) and to global overturning along openings (Fig. 10c and d). The fragility curves for the categories of the two-story buildings, prone to partial overturning are reported in Fig. 11 (Fig. 11a for "MUR 1" and Fig. 11b for "MUR 2"). Figure 12 shows the fragility curves for the categories of the three-story buildings, prone to global overturning (Fig. 12a) for "MUR 1" and b for "MUR 2" and to global overturning along openings (Fig. 12c) for "MUR 1" and d for "MUR 2". Lastly, Fig. 13 shows the fragility curves for the categories of the three-story buildings, prone to partial overturning at the third floor (Fig. 13a) for "MUR 1" and b for "MUR 2", and to partial overturning of the second and third floor (Fig. 13c) for "MUR 1" and Fig. 13d for "MUR 2".

Comparing among them the curves obtained by considering the smooth code-based spectra and the ones obtained from the recorded accelerograms, it emerges the influence of the modelling dispersion and the conditional mean value.

In particular, it is possible to observe that, while for the case of the two-story buildings prone to global overturning, the greatest scatter between DS_R and DN_R corresponds to MUR 1 (see Fig. 10), for the cases of the two-story buildings prone to partial overturning (Fig. 11) and the three-story buildings prone to global overturning and the global overturning along openings (Fig. 12), a greater scatter between the two curves occurs in the case of MUR 2. Finally, for the cases of the three-story buildings prone to partial overturning at the third floor and to partial overturning at the second and third floor (Fig. 13) the fragility curves are coincident. The scatter observed between some of the obtained curves is mainly dependent on the values of the modelling dispersion and the conditional mean. Indeed, for these cases, these parameters differ among them because of the difference between the value of the maximum displacement demand obtained by the smoothed spectra and the one deduced from natural spectra. The latter, indeed, may differ from the smoothed ones within a range of -10% and $+30\%$.

The variability of σ_{rtrDSi} depends moreover on the damage limit state (DS1 or DS2) and the floor where the failure mode activates (ground floor or upper levels); in particular:

- For DS1, the dispersion due to the record-to-record variability is in the range 0.25–0.39 for the failure modes activating at the ground floor, i.e. global overturning and overturning along openings, while it is in the range 0.16–0.32 for the failure modes involving a partial number of floor (Table 4);
- For the DS2, the dispersion due to the record-to-record variability is in the range 0.55–0.66 for the failure modes activating at the ground floor, i.e. global overturning and overturning along openings, while it is in the range 0.19–0.28 for the failure modes involving a partial number of floors (Table 4).

This variability is due to the fact that the period employed to determine the maximum displacement demand, through the CSM, varies with the variation of the damage limit state and of the floor where the failure mode activates. As a result, damage indices and the corresponding the dispersion σ_{rtrDSi} vary.

By comparing the curves of Figs. 10 and 12 to those of Figs. 11 and 13, it is evident that the buildings subjected to global overturning (Fig. 10 and 12) are more vulnerable than those affected by partial overturning (Fig. 11 and 13), both considering the curves obtained with spectra derived by natural records DS1(2)_R and the ones obtained with smoothed spectra DS1(2)_N; this highlights the great benefit of inserting structural details able to avoid the global overturning of the walls.

4 Conclusions and future developments

The work proposed in this paper is part of a research activity undertaken by the Authors and concerning the development of a methodology for a large-scale assessment of the seismic vulnerability of URM buildings in historic towns; the methodology could be helpful to identify the buildings that need priority of interventions with the aim of improving the seismic safety of historic centers and safeguarding their building heritage. In particular, the paper has proposed an approach for evaluating the fragility curves of URM buildings susceptible to OOP failure modes, which, starting from some previous works by the Authors (Cima et al. 2021b, a, 2023), accounts also for the record-to-record variability, by using spectrum-compatible natural records. In this context, the study presented in this paper has been finalized to investigate the influence of the type of the seismic input (smooth code-based spectra or spectra derived from a set of spectrum-compatible recorded accelerograms) adopted for deriving the seismic demand.

A central issue of the approach is represented by the knowledge, in terms of both geometry and mechanical features as well as the construction and structural details, of the buildings characterizing the area under study. Indeed, the proposed approach combines a survey process concerning the typological and the structural features of the buildings with the numerical derivation of the fragility curves throughout an integrated multistep procedure. The input data can be deduced from available databases and this aspect certainly represents a strength of the presented approach, which can be therefore usefully applied to any historic centre.

It is worth pointing out that the proposed approach represents an innovative tool since it allows to derive the curves in function of the OOP failure mode that has the greatest probability of being activated in the building, detected on the basis of a preliminary knowledge process. In addition, the approach estimates the fragility curves with reference to two distinct damage states, representative of two performances of the OOP failure modes: the activation of the failure mode for the achievement of the Damage Limit State and the collapse due to the achievement of the Safeguard Life Limit State, in compliance to the current Italian guidelines (ISR 2019).

With reference to the case study of Sora, the procedure has been applied starting from the data obtained from a survey analysis made by the authors within the Project DPC/ReLUIS 20192-2021 and available within the CARTIS database (Zuccaro et al. 2023). In order to analyze the influence of the type of the adopted spectral shapes, the fragility curves have been derived by adopting both the smoothed spectral shapes proposed by the Italian Codes and the natural spectral shapes derived by combinations of natural accelerograms. The analyses have highlighted that it is possible to obtain consistent fragility curves by employing the smooth code-based spectra, in compliance to the Italian Code, provided that an adequate value of the dispersion σ_{rtrDSi}, derived on natural records, is considered for the evaluation of the total dispersion of the curves. The values of the record-to-record

dispersions obtained by using the natural spectra suggests that these dispersions vary in ranges that are function of both the damage limit state and the level with respect to the ground where the failure mode activates (ground floor or upper floors). Consequently, the damage limit state and the level where the failure mode activates could be parameters that drive the choice of the most appropriate value of the record-to-record dispersion to consider within the evaluation of the seismic demand directly through the smooth code-based spectra. Moreover, the obtained fragility curves have evidenced that the buildings subjected to global overturning are more vulnerable than those susceptible to partial overturning.

Further developments of the approach will concern the extension to URM buildings in aggregate configuration by considering other aspects not yet included in this study such as the presence of double facing walls which often characterize masonry buildings, as well as the effect on the OOP failure modes of the mutual interaction among adjacent structural units under seismic action (Cima et al. 2022a, b; Moretić et al. 2023), which is certainly one of the main peculiarities of historic centres.

Author contributions Conceptualization: VC, VT, EG and MI; Methodology: VC, VT, EG and MI; Formal analysis and investigation, VC, VT, EG and MI; Writing—original draft preparation, VC and VT; Writing—review and editing: VC, VT, EG and MI; Funding acquisition, MI; Resources: VC, VT; Supervision: EG and MI. All authors read and approved the final manuscript.

Funding This study was funded by "Project DPC/ReLUIS 2022–2024—WP2. Inventory of existing structural and building typologies—CARTIS".

Data availability The datasets generated during and/or analysed during the current study are available from the corresponding author on reasonable request.

Declarations

Conflict of interest The authors have no relevant financial or non-financial interests to disclose.

References

Abbati SD, Cattari S, Lagomarsino S (2018) Theoretically-based and practice-oriented formulations for the floor spectra evaluation. Earthq Struct. https://doi.org/10.12989/eas.2018.15.5.565

Ahmad N, Ali Q (2017) Displacement-based seismic assessment of masonry buildings for global and local failure mechanisms. Cogent Eng 4:1414576

Applied Technology Council (2012) FEMA P-58-4: seismic performance assessment of buildings. Fema P-58-4

Banerjee AK, Pramanik D, Roy R (2016) Seismic structural fragilities: Proposals for improved methodology per spectral matching of accelerogram. Eng Struct 111:538–551. https://doi.org/10.1016/J.ENGSTRUCT.2016.01.002

Baraschino R, Baltzopoulos G, Iervolino I (2020) R2R-EU: software for fragility fitting and evaluation of e stimation uncertainty in seismic risk analysis. Soil Dyn Earthq Eng 132:106093. https://doi.org/10.1016/J.SOILDYN.2020.106093

Biglari M, Formisano A (2020) Damage probability matrices and empirical fragility curves from damage data on masonry buildings after Sarpol-e-zahab and bam earthquakes of Iran. Front Built Environ 6:2

Blandon CA, Priestley MJN (2005) Equivalent viscous damping equations for direct displacement based design. J Earthq Eng 9:257–278

Brando G, De Matteis G, Spacone E (2017) Predictive model for the seismic vulnerability assessment of small historic centres: Application to the inner Abruzzi Region in Italy. Eng Struct. https://doi.org/10.1016/j.engstruct.2017.10.013

Calvi G (1999) A displacement-based approach for vulnerability evaluation of classes of buildings. J Earthq Eng 3:411–438

Candela M, Cattari S, Lagomarsino S, Fonti R (2013) Prove in situ per la caratterizzazione della muratura in pietrame grezzo alle azioni nel piano e fuori dal piano. In: Proceedings of the Conference of the Italian National Association of Earthquake Engineering (ANIDIS), Padua, Italy. pp 1–10

Carocci CF (2012) Small centres damaged by 2009 L'Aquila earthquake: on site analyses of historical masonry aggregates. Bull Earthq Eng. https://doi.org/10.1007/s10518-011-9284-0

Casapulla C, Argiento LU (2017) Non-linear kinematic analysis of masonry walls out-of-plane loaded. The comparative role of friction between interlocked walls. In: COMPDYN 2017—Proceedings of the 6th International Conference on Computational Methods in Structural Dynamics and Earthquake Engineering

Chieffo N, Formisano A (2019) Comparative seismic assessment methods for masonry building aggregates: a case study. Front Built Environ 5:123

Chieffo N, Formisano A (2020) Induced seismic-site effects on the vulnerability assessment of a historical centre in the Molise Region of Italy: analysis method and real behaviour calibration based on 2002 earthquake. Geosciences (basel) 10:21

Chieffo N, Clementi F, Formisano A, Lenci S (2019) Comparative fragility methods for seismic assessment of masonry buildings located in Muccia (Italy). J Build Eng. https://doi.org/10.1016/j.jobe.2019.100813

Chieffo N, Formisano A, Landolfo R, Milani G (2022) A vulnerability index based-approach for the historical centre of the city of Latronico (Potenza, Southern Italy). Eng Fail Anal 136:106207. https://doi.org/10.1016/j.engfailanal.2022.106207

Cima V, Tomei V, Grande E, Imbimbo M (2021b) Fragility curves at regional basis for unreinforced masonry buildings prone to out-of-plane mechanisms: the case of Central Italy. Structures 34:4774–4787. https://doi.org/10.1016/j.istruc.2021.09.111

Cima V, Bartolomeo C, Grande E, Imbimbo M (2022a) Natural fibers for out-of-plane strengthening interventions of unreinforced masonry buildings in aggregate configuration. Sustainability 14:9967

Cima V, Tomei V, Grande E, Imbimbo M (2023) Fragility curves for residential unreinforced masonry buildings prone to out-of-plane mechanisms: the case of the historical center of Sora. Proc Struct Integr 44:211–218. https://doi.org/10.1016/j.prostr.2023.01.028

Cima V, Tomei V, Grande E, Imbimbo M (2021a) Seismic vulnerability of Italian historical towns: the case of Borgo San Rocco. In: Advances in science and technology, proceedings of the 22nd conference on the rehabilitation and reconstruction of buildings. Trans Tech Publications Ltd, pp 1–7

Cima V, Bartolomeo C, Grande E, Imbimbo M (2022b) Influence of the aggregate effect on the seismic vulnerability of Italian historical centers. In: Proceedings of the International Conference on Knowledge Transfer on Sustainable Rehabilitation and Risk Management in the Built Environment—KNOW-RE-BUILT—p (in press)

CNR-DT212 (2013) Recommendations for the probabilistic seismic assessment of existing buildings (in Italian)

Columbro C, Eudave RR, Ferreira TM et al (2022) On the use of web mapping platforms to support the seismic vulnerability assessment of old urban areas. Remote Sens (basel) 14:1424

D'Ayala D, Meslem A, Vamvatsikos D, et al (2015) Guidelines for analytical vulnerability assessment: low/mid-rise, GEM vulnerability and loss modelling. Global Earthquake Model (GEM) Foundation, Pavia

D'Ayala D, Speranza E (2003) Definition of collapse mechanisms and seismic vulnerability of historic masonry buildings. Earthq Spectra 19:479–509. https://doi.org/10.1193/1.1599896

Donà M, Carpanese P, Follador V et al (2020) Mechanics-based fragility curves for Italian residential URM buildings. Bull Earthq Eng 19:3099–3127. https://doi.org/10.1007/S10518-020-00928-7

European Commitee for Standardization (2004) Eurocode 8: design of structures for earthquake resistance—Part 1 : general rules, seismic actions and rules for buildings. European Committee for Standardization

Formisano A (2017) Theoretical and numerical seismic analysis of masonry building aggregates case studies in San Pio Delle Camere (L'Aquila, Italy). J Earthq Eng. https://doi.org/10.1080/13632469.2016.1172376

Freeman SA (1998) The capacity spectrum method as a tool for seismic design. In: 11th European conference on earthquake engineering

Giordano N, De Risi R, Voyagaki E, et al (2021) Seismic fragility models for typical non-engineered URM residential buildings in Malawi. In: Structures. Elsevier, pp 2266–2278

Giuffré A (1993) Sicurezza e conservazione dei centri storici. Il caso di Ortigia. Laterza, Bari

Heyman J (2014) The stone skeleton: Structural engineering of masonry architecture

Iervolino I, Galasso C, Cosenza E (2010) REXEL: computer aided record selection for code-based seismic structural analysis. Bull Earthq Eng. https://doi.org/10.1007/s10518-009-9146-1

ISR (Italian Seismic Recommendations) (2019) Circolare 21 gennaio 2019 n.7: Istruzioni per l'applicazione dell'«Aggiornamento delle "Norme Tecniche per le Costruzioni"» di cui al decreto

ministeriale 17 gennaio 2018. Supplemento ordinario alla "Gazzetta Ufficiale" n 35 dell'11 febbraio 2019—Serie generale (in Italian)
Jalayer F, De Risi R, Manfredi G (2015) Bayesian cloud analysis: efficient structural fragility assessment using linear regression. Bull Earthq Eng. https://doi.org/10.1007/s10518-014-9692-z
Jalayer F, Ebrahimian H, Miano A (2021) Record-to-record variability and code-compatible seismic safety-checking with limited number of records. Bull Earthq Eng 19:6361–6396. https://doi.org/10.1007/S10518-020-01024-6/TABLES/3
Lagomarsino S (2015) Seismic assessment of rocking masonry structures. Bull Earthq Eng. https://doi.org/10.1007/s10518-014-9609-x
Lagomarsino S, Resemini S (2009) The assessment of damage limitation state in the seismic analysis of monumental buildings, Earthquake Spectra. https://doi.org/10.1193/1.3110242
Lagomarsino S, Cattari S (2014) Fragility functions of masonry buildings. Geotech Geol Earthq Eng. https://doi.org/10.1007/978-94-007-7872-6_5
Liguori FS, Fiore S, Perelli FL, et al (2023) A mechanical-based seismic vulnerability assessment method with an application to masonry structures in Cosenza (Italy). Bull Earthq Eng 1–27
Lourenço PB, Mendes N, Ramos LF, Oliveira DV (2011) Analysis of masonry structures without box behavior. Int J Archit Herit. https://doi.org/10.1080/15583058.2010.528824
Moretić A, Chieffo N, Stepinac M, Lourenço PB (2023) Vulnerability assessment of historical building aggregates in Zagreb: implementation of a macroseismic approach. Bull Earthq Eng 21:2045–2065
Mosoarca M, Onescu I, Onescu E et al (2019) Seismic vulnerability assessment for the historical areas of the Timisoara city, Romania. Eng Fail Anal 101:86–112
Nale M, Minghini F, Chiozzi A, Tralli A (2021) Fragility functions for local failure mechanisms in unreinforced masonry buildings: a typological study in Ferrara, Italy. Bull Earthq Eng. https://doi.org/10.1007/s10518-021-01199-6
Nettis A, Gentile R, Raffaele D et al (2021) Cloud capacity spectrum method: accounting for record-to-record variability in fragility analysis using nonlinear static procedures. Soil Dyn Earthq Eng 150:106829
Nielson BG, DesRoches R (2007) Seismic fragility methodology for highway bridges using a component level approach. Earthq Eng Struct Dyn. https://doi.org/10.1002/eqe.655
NTC18 (2018) Norme Tecniche per le Costruzioni. DM 17/1/2018. Italian Ministry of Infrastructure and Transport
Park J, Towashiraporn P, Craig JI, Goodno BJ (2009) Seismic fragility analysis of low-rise unreinforced masonry structures. Eng Struct 31:125–137
Pelà L (2018) New trends and challenges in large-scale and urban assessment of seismic risk in historical centres. Int J Archit Herit 12:1051–1054
Penna A, Morandi P, Rota M et al (2014) Performance of masonry buildings during the Emilia 2012 earthquake. Bull Earthq Eng 12:2255–2273
Protezione Civile (2017) Manual for the compilation of the 1° level form for the typological-structural characterization of urban sectors consisting in ordinary buildings
Rapone D, Brando G, Spacone E, De Matteis G (2018) Seismic vulnerability assessment of historic centers: description of a predictive method and application to the case study of scanno (Abruzzi, Italy). Int J Archit Herit. https://doi.org/10.1080/15583058.2018.1503373
Rosti A, Rota M, Penna A (2021) Empirical fragility curves for Italian URM buildings. Bull Earthq Eng. https://doi.org/10.1007/s10518-020-00845-9
Saccucci M, Cima V, Grande E, Imbimbo M (2019) Valutazione della vulnerabilità sismica degli aggregati in muratura: il caso di Borgo San Rocco a Sora (Italia). In: Proceedings of the XVIII ANIDIS conference seismic engineering in Italy: Ascoli Piceno, 15–19 September 2019. Press, Pisa University, pp 152–162
Saccucci M, Cima V, Grande E, Imbimbo M (2021) The knowledge process in the seismic assessment of masonry building aggregates—An Italian case study. In: Rotaru A (ed) International conference on critical thinking in sustainable rehabilitation and risk management of the built environment. Springer, Cham, pp 330–347
Saccucci M (2020) Analisi multilivello BIM per la valutazione della vulnerabilità sismica degli edifici in muratura (In Italian)
Sandoli A, Lignola GP, Calderoni B, Prota A (2021) Fragility curves for Italian URM buildings based on a hybrid method. Bull Earthq Eng. https://doi.org/10.1007/s10518-021-01155-4
Sandoli A, Calderoni B, Lignola GP, Prota A (2022) Seismic vulnerability assessment of minor Italian urban centres: development of urban fragility curves. Bull Earthq Eng. https://doi.org/10.1007/S10518-022-01385-0

Scaini C, Peresan A, Tamaro A et al (2022) Can high-school students contribute to seismic risk mitigation? Lessons learned from the development of a crowd-sourced exposure database. Int J Disaster Risk Reduct 69:102755

Shabani A, Kioumarsi M, Zucconi M (2021) State of the art of simplified analytical methods for seismic vulnerability assessment of unreinforced masonry buildings. Eng Struct 239:112280

Silva V, Akkar S, Baker J et al (2019) Current challenges and future trends in analytical fragility and vulnerability modeling. Earthq Spectra 35:1927–1952

Simões AG, Bento R, Lagomarsino S et al (2020) Seismic assessment of nineteenth and twentieth centuries URM buildings in Lisbon: structural features and derivation of fragility curves. Bull Earthq Eng 18:645–672

Sorrentino L, Cattari S, da Porto F et al (2019) Seismic behaviour of ordinary masonry buildings during the 2016 central Italy earthquakes. Bull Earthq Eng. https://doi.org/10.1007/s10518-018-0370-4

Tocchi G, Polese M, Di Ludovico M, Prota A (2022) Regional based exposure models to account for local building typologies. Bull Earthq Eng 20:193–228. https://doi.org/10.1007/s10518-021-01242-6

Vlachakis G, Vlachaki E, Lourenço PB (2020) Learning from failure: damage and failure of masonry structures, after the 2017 Lesvos earthquake (Greece). Eng Fail Anal 117:104803

Zuccaro G, Dolce M, Perelli FL et al (2023) Cartis: a method for the typological-structural characterization of Italian ordinary buildings in urban areas. Front Built Environ 9:1129176

Zuccaro G, Rauci M (2008) Collapse mechanisms of masonry structures: From the identification of vulnerability factors to the safety check and retrofitting. In: AIP conference proceedings

Zuccaro G, Dolce M, De Gregorio D, et al (2015) La scheda CARTIS per la caratterizzazione tipologico-strutturale dei comparti urbani costituiti da edifici ordinari. Valutazione dell'esposizione in analisi di rischio sismico. In: Proceedings of the GNGTS

Publisher's Note Springer Nature remains neutral with regard to jurisdictional claims in published maps and institutional affiliations.

Springer Nature or its licensor (e.g. a society or other partner) holds exclusive rights to this article under a publishing agreement with the author(s) or other rightsholder(s); author self-archiving of the accepted manuscript version of this article is solely governed by the terms of such publishing agreement and applicable law.